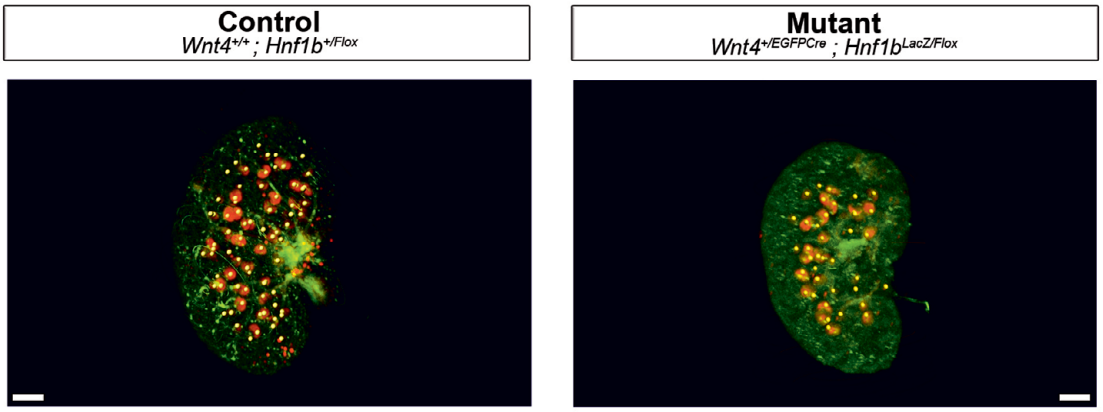

Fig. S1. Mutant mouse kidneys have fewer glomeruli than controls. The glomeruli were identified using an anti-nephrin antibody (red), while autofluorescence of the tissue served to depict the overall shape of the kidney (green). Comparison of nephrin immunostaining in the kidneys of control and mutant embryos demonstrates a notable reduction in the amount of glomeruli in the mutant. The yellow dots were generated by the Imaris software and were used for quantification of the glomeruli. Note that the glomeruli are more compact at in the medulla of the mutant kidney than in the control.

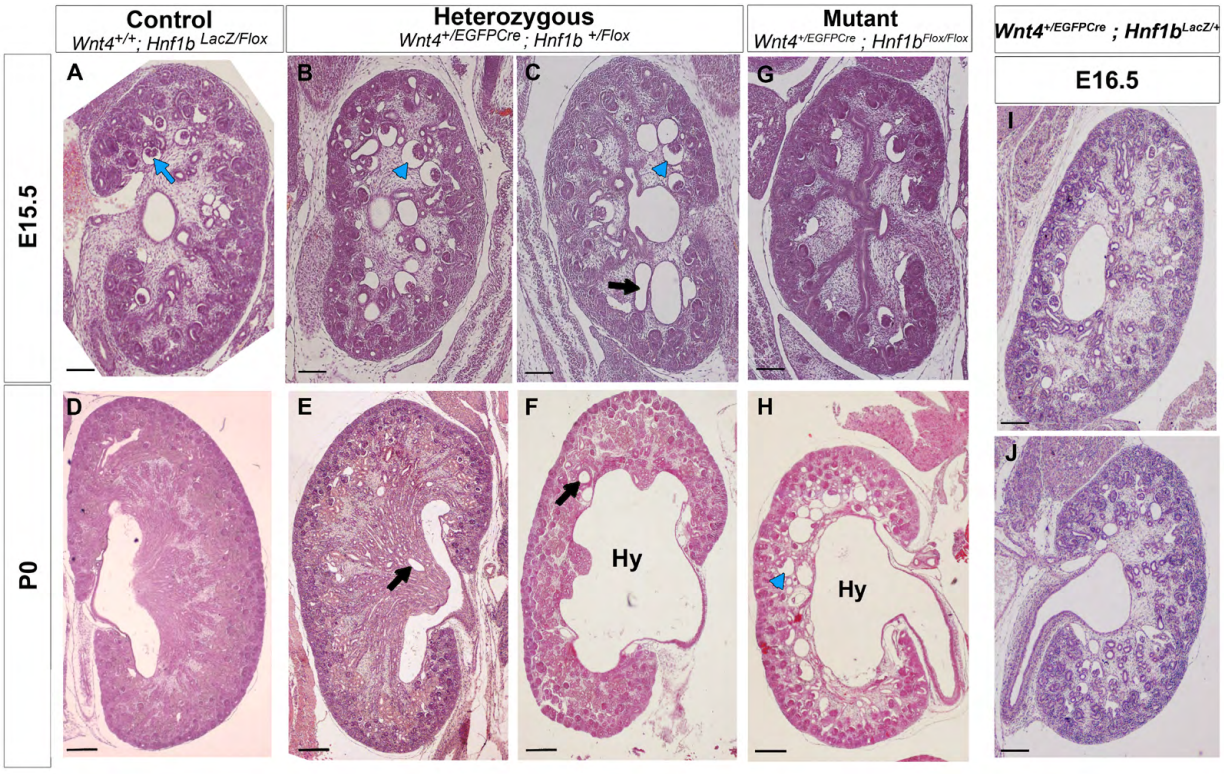

Fig. S2. Comparative kidney histology of *Hnf1b* mutants and compound heterozygotes *Wnt4*$^{+/EGFPCre}$; *Hnf1b*$^{+/Flox}$ and *Wnt4*$^{+/EGFPCre}$; *Hnf1b*$^{lacZ/+}$. Hematoxylin-Eosin staining of control, heterozygous and mutant mouse kidneys at several stages. (**A-H**) Part of compound heterozygous *Wnt4*$^{+/EGFPCre}$; *Hnf1b*$^{+/Flox}$ kidneys displays cystic glomeruli (blue arrowhead) and enlarged tubules (black arrow) at E15.5. Hydronephrosis (Hy) is occasionally observed at P0 in both heterozygotes and mutants. (**I**,**J**) *Wnt4*$^{+/EGFPCre}$; *Hnf1b*$^{lacZ/+}$ compound heterozygotes have no phenotype at E16.5, implying that the phenotype observed for the *Wnt4*$^{+/EGFPCre}$; *Hnf1b*$^{+/Flox}$ compound heterozygote was not the consequence of genetic interaction between *Wnt4* and *Hnf1b* due to decreased levels of both genes. Furthermore, *Wnt4* transcripts assayed by qRT-PCR or ISH were similar in *Wnt4*$^{+/EGFPCre}$ and mutants, indicating that HNF1B does not control *Wnt4* expression. Scale bars: 200 µm.

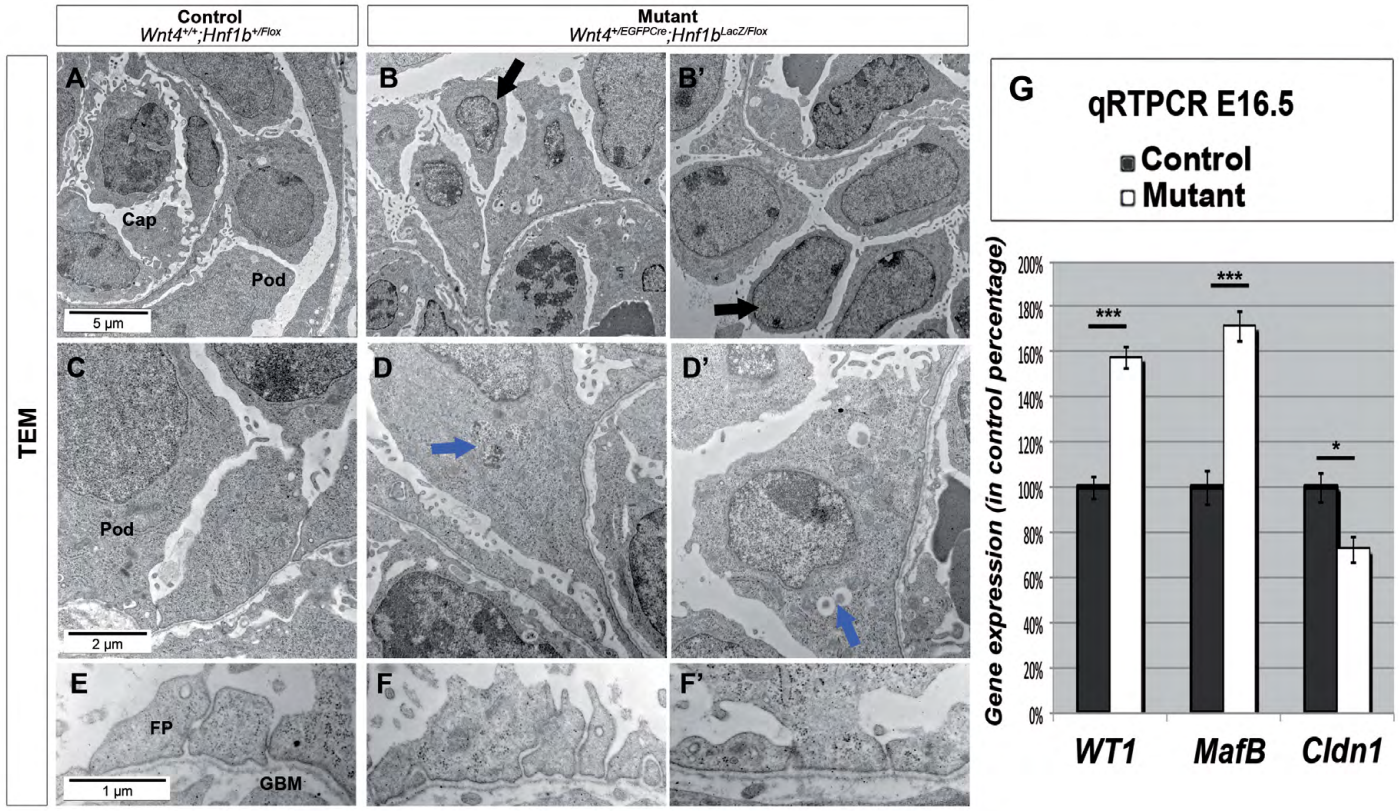

Fig. S3. Mutant glomeruli display a transient disorganisation of podocytes. (**A-F′)** Ultrastructure analysis of E16.5 mouse kidneys by electron microscopy showed that mutant podocytes make normal foot processes (FP) on the glomerular basal membrane (GBM). However, some mutant podocytes (Pod) present numerous vesicles (blue arrow) and occasionally appear detached from the GBM (black arrow), probably explaining the thicker appearance of the podocyte layer compared with controls (A-D′). (**G**) The increase in transcript levels of the podocyte markers *Wt1* and *Mafb* of 63.4% and 71.6%, respectively, compared with control littermates may be in part related to the thickness of the podocyte layer. Note that the transcript level of the Bowman's capsule marker *Cldn1* is reduced in the mutant (by 27.5%).

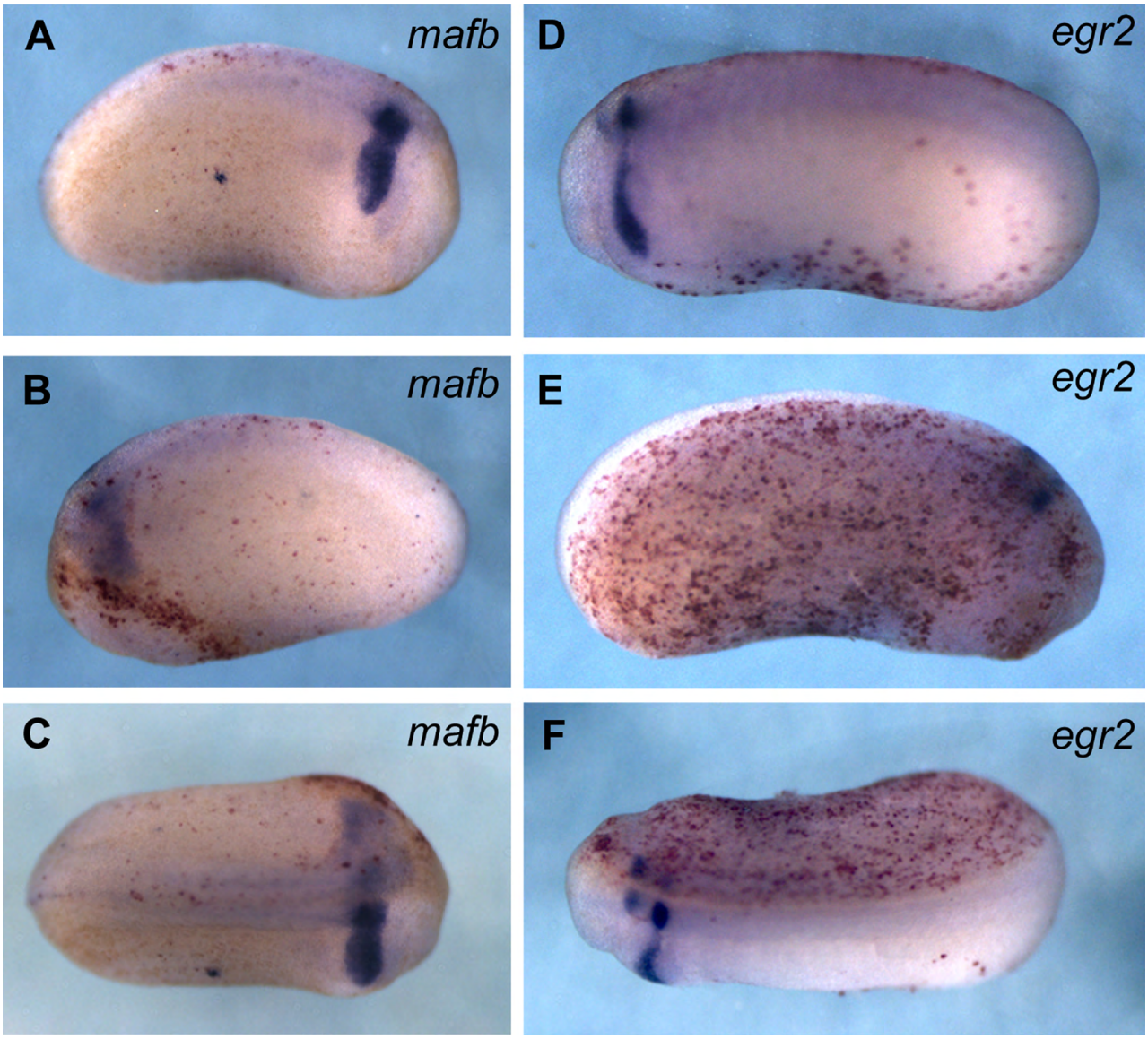

Fig. S4. Expression of HNF1B-DN leads to hindbrain segmentation defects. Decreasing HNF1B-DN mRNA quantities were injected at the 4-cell stage. At either 250 or 500 pg, the vast majority of the embryos were abnormal, with an open blastopore or a body curved towards the injected side, whereas at either 125 pg or 65 pg, more than 80% of tadpoles were similar to controls. In all experiments we therefore used 65 pg and 125 pg and only those tadpoles with normal morphology were considered for further analysis. (**A-F**) Whole-mount ISH of *Xenopus* embryos injected at the 8-cell stage in two animal blastomeres with HNF1B-DN and *lacZ* mRNAs and analysed at stage 23 for *mafb* (A-C) and stage 25 for *egr2* (D-F). The injected side is revealed by β-gal staining (red). (A,B,D,E) Lateral views; (C,F) dorsal views. Expression of *egr2* in r5 and r5-derived neural crest is strongly inhibited in the presence of HNF1B-DN. Similarly, HNF1B-DN decreases *mafb* expression in r4 and r5.

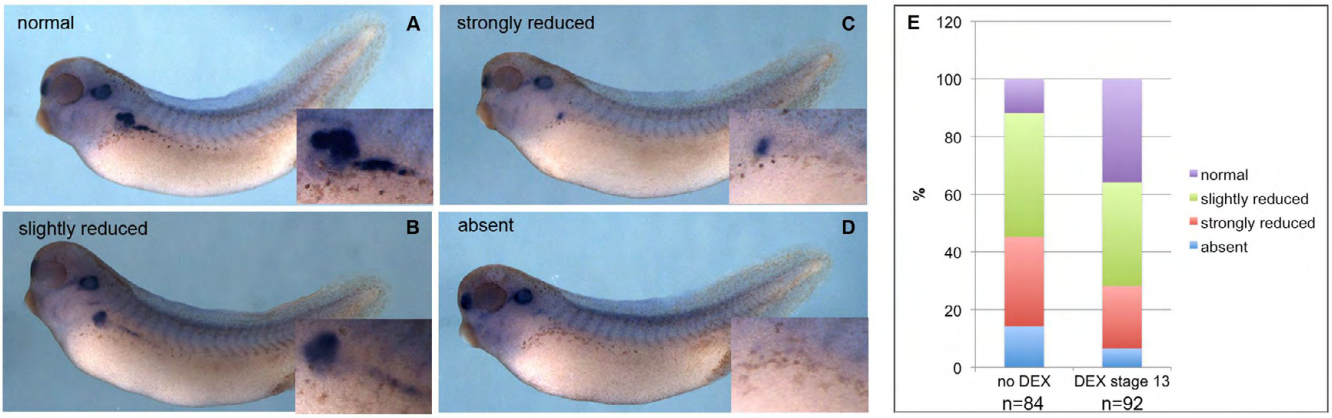

Fig. S5. Pronephros defects caused by dominant-negative HNF1B-DN are partially rescued by *Irx1*. (**A-D**) Four-cell stage *Xenopus* embryos were co-injected with HNF1B-DN mRNA (150 pg) and Irx1-GR mRNA (500 pg), incubated or not in dexamethasone (DEX) at early neurula stage 13 and analysed for *slc4a4* expression by ISH at stage 35. Phenotypes were classified into four categories: normal (A), slightly reduced (B), strongly reduced (C) and absent (D). Insets show a higher magnification of the anterior pronephric territory. (**E**) Quantification of the results for six independent experiments. *n*, number of embryos analysed.

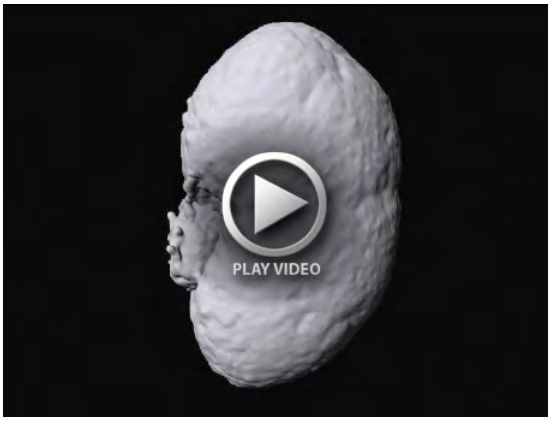

Movie 1

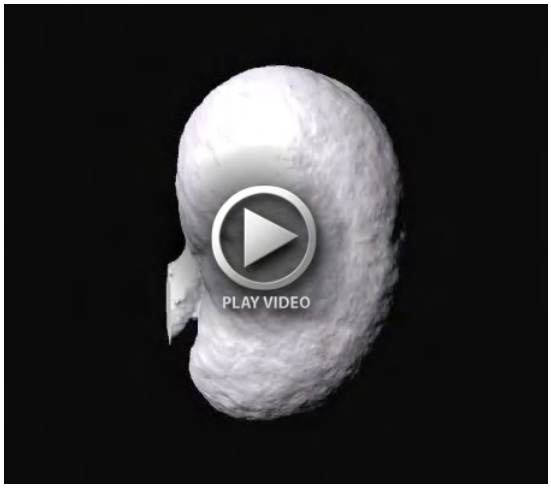

Movies 1 and 2. Mature glomeruli count from OPT analysis of control (Movie 1) and mutant (Movie 2) kidneys. The OPT imaging generates a stack of figures that were taken sequentially around the kidney. These were aligned together to produce tomographic sections and movies. The results presented as snapshots in Fig. S1 of the control and mutant mouse kidney at E15.5 are depicted here in the OPT movies. Movies indicate the maturing glomeruli (red) followed by the appearance of yellow dots generated by Imaris software highlighting the quantified glomeruli. Compare Movie 2 with Movie 1.

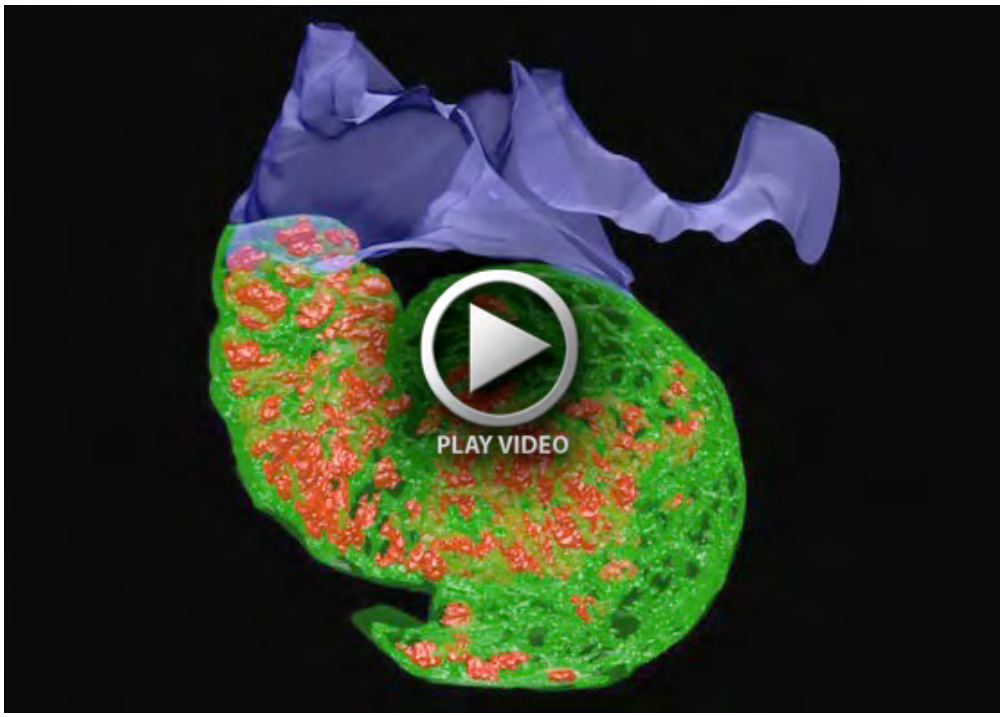

Movie 3

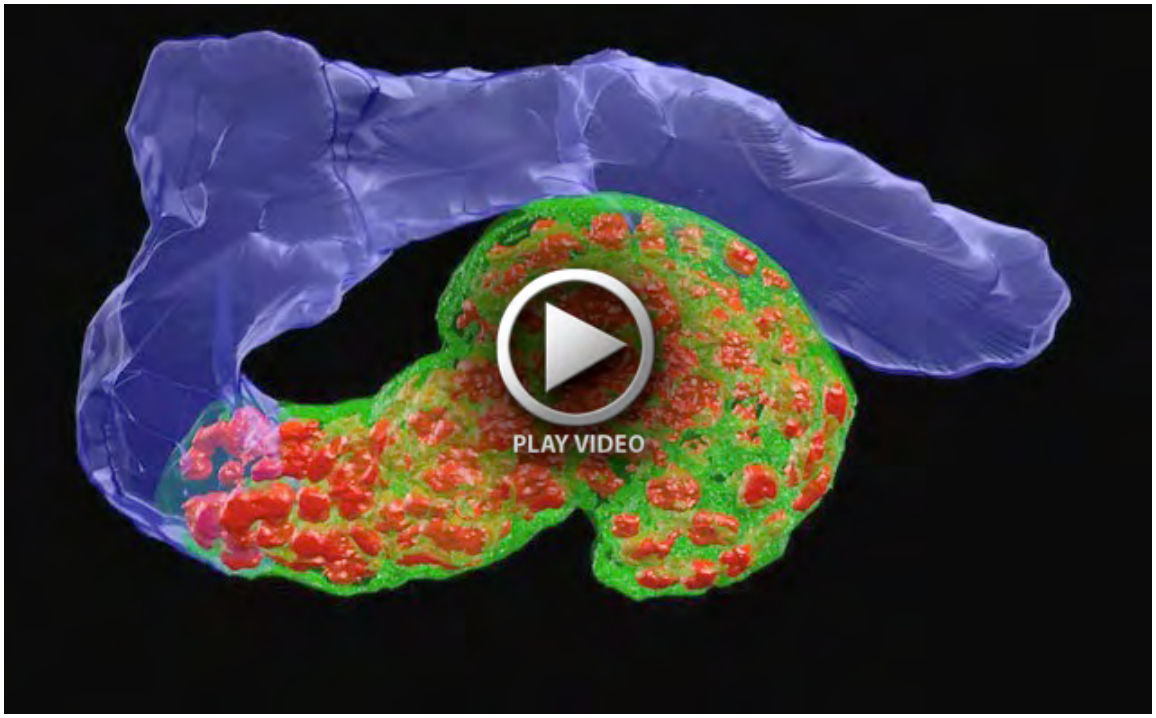

Movies 3 and 4. High-resolution 3D reconstructions of control (Movie 3) and mutant (Movie 4) SSBs. Based on β-catenin membrane labelling, we reconstructed in 3D the collecting duct (false coloured in purple) and the SSB shape using IMOD software. Isosurfaces of the β-catenin staining were used to visualise cell membranes within the SSB. Isosurfaces of PAX2 staining were added into the membrane object and the detection threshold was fixed to only detect the distal and intermediate part, where PAX2 was strongest in control SSB, in order to help to visualise the SSB convoluted shape. Note that only a few nuclei were stained in the future proximal territory (close to the collecting duct trunk) and in the developing glomerulus. In the mutant, SSB shape is clearly less convoluted. Using the same threshold as in the control for PAX2 detection, we also confirmed the maintenance of its expression in the entire proximal part of the SSB. Model and staining files were then imported into Blender software to generate the movies.

Table S1. Oligonucleotides

Target	Forward (5'→3')	Reverse (5'→3')	Position
Oligonucleotides for qRT-PCR			
Cyclophilin A	CAGGTCCTGGCATCTTGTCC	TTGCTGGTCTTGCCATTCCT	319 / 503
Cdh6	TCCCGGAGATGGCTGATGTT	GCATCAGTCGCCGTGACTTG	762 / 816
Dll1	GCCCTCCATACAGACTCTCCC	AGGCGGCTGATGAGTCTTTCT	958 / 1020
Hes1	CAAAGACGGCCTCTGAGCAC	CCTTCGCCTCTTCTCCATGAT	317 / 375
Hes5	CTCCGCTCGCTAATCGCCTC	TCTCCACCGCCACGGTACTT	41 / 101
Hey1	TCACCTGAAAATGCTGCACAC	CGTGCGCGTCAAAATAACCT	465 / 517
Hnf1b wild type	GGCCTACGACCGGCAAAAGA	GGGAGACCCCTCGTTGCAAA	925 / 1020
Hnf4a	CCATCATCTTCTTTGATCCAG	CTCACTTGCACCTGTGACC	989 / 1070
Irx1	TTATCCCTATGGTCAGTTTCAATACG	CGTTGAGCCAGGCTTTCAG	586 / 677
Irx2	GCATTCACTGGAGTCCCACT	ACAACTGCACAGCCCTCACT	1401 / 1481
Irx3	CAACGAGCACCGCAAGAA	TGGTGATGATGGCCAACATG	581 / 645
Jag1	TGCCCTCCAGGACATAGTGG	ACTCTCCCCATGGTGATGCA	2610 / 2680
Lfng	CTCGCGCCACAAGGAGATGAC	CCGAGGAGCAGTTGGTGAGCA	486 / 583
Mafb	AACTCGCCAACTCCGGCTTC	ACCCGCCAGGACTCACAGAA	1288 / 1373
Notch1	AACACCGCCCGTGGATTCAT	ACATGTGGCACCCTCGAAGC	4243 / 4299
Notch2	CCTGCCAGGTTTTGAAGGGA	GGGCAGTCGTCGATATTCCG	905 / 955
Osr2	ACAACAGCACGCAGGAAT	GCCGAAAAAGAAGTTCTC	40/171
Papss2	ACTGCAAAGCACCCCCATATC	CCAACAAGCCAGTCCCCACT	1215 / 1270
Pax2	GGGCATCTGCGATAATGACA	GGTCCGGATGATCCTGTTGAT	360 / 420
Pcsk9	AGGAGCATGGGATCTCAGGTC	TGCATCCAGTCAGGGTCCA	2256 / 2330
Tcfap2b	GCAGTCAGTTGAAGATGCCA	AGTCACAGATTTGGGAGGGA	95/185
Sox9	AAGCCGACTCCCCACATTCCTC	CGCCCCTCTCGCTTCAGATCAA	569 / 695
Wfdc2	CGGCAGAAACAACCTCCT	CAATGGATGTGGGAAGATGG	107/197
Wt1	GGTCTTCCGAGGCATTCAGG	CTGACCGGACAAGAGTTGGG	1348 / 1412
Oligonucleotides for ChIP-qPCR			
Dll1 s-5917	TGGCACAATGAGAGGCTTTTG	TTAAACAGCCCGGTGCTCTG	–5875 / –5953
Irx1-2 s-430229	CATCGCCAGCTCCTGATACG	CGGTGGGCACGGTTAATCATTT	–430267 / –430212*
Irx1-2 s-418342	CTGGCTGACAAGAAGAAGTGAACG	TACGGCCTGATACCAACATGG	–418410 / –418355*
Irx2 -500/+50	AGATGAGAGTGTGACGGACAGC	CGAGTTTCCGAGGGACATTG	–231 / –181
Lfng s-4173	CTGAGAGCTGGCACCCTTACC	TTGGGTCCCCTGTCATTTTGT	–4261 / –4211
Hnf4a s-6252	CAGGGTTAGGGGTGAGACAA	CCTCCCTGTCCTCAGTGTGA	–6295 / –6173

*With respect to the *Irx2* TSS.